

## Article

# Analysis of Shell Egg Pasteurization Using Computational Fluid Dynamics

Pavlos-Antonios Sampanis, Stylianos M. Chatzidakis, George N. Stoforos and Nikolaos G. Stoforos \* 

Department of Food Science and Human Nutrition, Agricultural University of Athens, 11855 Athens, Greece; pavlos.sabanis@gmail.com (P.-A.S.); chatzidakis.stelios@gmail.com (S.M.C.); georgestof@gmail.com (G.N.S.)

\* Correspondence: stoforos@aua.gr; Tel.: +30-210-529-4706

**Featured Application:** Thermal pasteurization remains the principal industrial method to ensure the safety of whole eggs and egg products. Using CFD simulations, this study reports time–temperature combinations to achieve the required 5-log reduction of *Salmonella enteritidis*.

**Abstract:** In the present work, the thermal pasteurization process of shell eggs was studied through Computational Fluid Dynamics. For large-size eggs (63–72 g), the required heating times at several different heating medium (water) temperatures, namely 54, 56, 58, and 60 °C (followed by cooling in water at 20 °C), were estimated as 55.1, 37.2, 29.1, and 24.5 min. Calculations were based on a 5-log reduction of the *Salmonella enteritidis* population, that is, for a target *F* value at 60 °C in 0.85 min. Computations were performed at the critical point of the egg, which was established from *F* value distribution determinations and was approximately located at the center of the yolk. Both heating and cooling cycle lethality was considered. Similar calculations were performed for medium (53–62 g) and extra-large-size eggs (>72 g). Microbial destruction occurring during the cooling cycle of the pasteurization process was greater for higher heating temperatures and larger egg sizes, ranging between 11.8% of the total destruction for the medium eggs heated at 54 °C and 72.9% for the extra-large eggs at a heating medium temperature of 60 °C. Therefore, destruction during the cooling cycle should not be ignored during the design of thermal pasteurization processes. For the kinetic parameters employed, quality degradation calculations revealed minimal changes for the processes investigated.



Academic Editor: Francesca Scargiali

Received: 13 December 2024

Revised: 20 January 2025

Accepted: 23 January 2025

Published: 26 January 2025

**Citation:** Sampanis, P.-A.; Chatzidakis, S.M.; Stoforos, G.N.; Stoforos, N.G. Analysis of Shell Egg Pasteurization Using Computational Fluid Dynamics. *Appl. Sci.* **2025**, *15*, 1263. <https://doi.org/10.3390/app15031263>

**Copyright:** © 2025 by the authors. Licensee MDPI, Basel, Switzerland. This article is an open access article distributed under the terms and conditions of the Creative Commons Attribution (CC BY) license (<https://creativecommons.org/licenses/by/4.0/>).

**Keywords:** thermal processing; *F* value; critical point; *Salmonella enteritidis*; CFD

## 1. Introduction

The egg is an essential part of the human diet, as it offers a combination of well-balanced, easily digestible nutrients. Eggs are a nutrient-dense food, providing essential lipids, high-quality proteins, vitamins, and minerals at a moderate calorie level (~140 kcal/100 g). They are an affordable source of key nutrients, including vitamin A, vitamin B12, iron, and choline, making them beneficial for overall health across all age groups [1]. However, fresh egg and its derived products have been declared potentially dangerous foods due to foodborne infections in cases of insufficient cooking or heat treatment [2,3]. The main reason is that *Salmonella enterica* can be found in the intestinal tract of the hen and from there it can pass to the egg, or it can be a result of perforation of the shell by the microorganism after egg-laying [4]. The United States Food and Drug Association requires a 5-log decimal reduction of the *Salmonella enterica* population for

thermal processing of eggs [2]. In the industry, the pasteurization process is applied to about only 1% of the eggs available in the market, and therefore eggs should be properly cooked by the consumer before consumption [5]. It is estimated that 1 in every 20,000 eggs produced in the United States is *Salmonella*-positive (0.005%) [6], while in Europe the frequency is higher at 0.37% [7]. Outbreaks due to *Salmonella* spp. are still a big issue for the food industry, with the latest outbreaks [8,9] impacting several countries and consumers, making whole egg pasteurization a necessary hazard step barrier. Implementing thermal pasteurization remains the principal industrial method to ensure the safety of eggs and egg products [5]. *Salmonella enterica* is the egg's most heat-resistant pathogen ( $D_{60^{\circ}\text{C}} = 0.17$  min,  $z$  value =  $4.08$  °C) [10,11]. The standard pasteurization method at  $57$  °C for 57.5 min might unnecessarily increase costs and affect product quality due to long heating time of the thermal process [12].

The pasteurization process makes the egg safer for the consumer; however, optimization of the process is necessary to ensure food safety without significant quality degradation. For many years, microbial destruction of *Salmonella enterica* has been extensively studied experimentally [5,12–14]; yet only recently, with the development and accessibility of computer simulation programs, has an increase in studies regarding optimizing the pasteurization process by studying and improving heat and mass transfer modeling been seen [11,15,16]. These studies, using Computational Fluid Dynamics (CFD), were able to simulate the temperature profile within whole eggs and calculate the time required to achieve the target lethality for *Salmonella enterica*. At this point, it is worth mentioning that CFD is a transformative tool in food processing, offering precision in modeling heat transfer, fluid dynamics, and mass transfer. It enables optimization of thermal processes like pasteurization and sterilization, enhancing food safety and quality while reducing energy use and experimental costs [17,18]. Using CFD simulation, studies on egg pasteurization were able to determine the slowest heating point (or zone) within the egg and design the process based on this as the worst-case scenario for food safety [11,15,16]. The slowest heating point within an intact egg was reported to be around the geometrical center of the egg samples [11,15]. Early studies examined the effects of the heat transfer coefficient between the heating medium and the egg surface on egg pasteurization [15]. Recently, a CFD study examined the heat and mass transfer of egg pasteurization and the efficiency of thermal treatment on *Salmonella enterica*, using the actual representation of intact egg components, such as eggshell, white, yolk, and air cells [11]. Abbasnezhad et al. [11], using a three-dimensional computational model, established the effects of eggshell thickness and the % of air cells in achieving target lethality.

All of the above-mentioned studies [11,15,16] restricted their analyses to the heating part of the pasteurization process. The cooling of the egg, which inevitably follows the heating cycle of the pasteurization process, is of equal importance in terms of microbial destruction, as at the initial stages of cooling the product is still at elevated temperatures. Microbial destruction occurring during the cooling cycle does not only affect the required heating time; it can also alter the position of the “cold spot”, the point inside of the egg that receives the least heat treatment and represents the critical point the pasteurization process should be based on. The cold spot does not necessarily coincide with the slowest heating point, and it can be assessed through lethality distribution calculations. Quality degradation during egg pasteurization is expected to be minimal, although quantitative calculations were not found.

Considering the above, this study aims to investigate the whole egg pasteurization process using CFD analysis. It follows a holistic approach, with the goals of the current work being the following: (1) to develop a three-dimensional heat transfer model for whole egg pasteurization, (2) to predict the time–temperature profile and the critical point location

based on experimentally determined heat transfer coefficients, (3) to estimate pasteurization efficiency ( $F$  values) considering microbial destruction at both the heating and the cooling cycle of the process, (4) to estimate quality degradation during pasteurization, and (5) to validate the theoretical model against experimental temperature data.

## 2. Materials and Methods

The thermal pasteurization of eggs was simulated using a multidimensional computational fluid dynamic model. The egg geometry was designed using 3D CAD (computer aided design) software (*Ansys DesignModeler, Release 22.1*, ANSYS, Inc., Canonsburg PA, USA) based on Euclidean Moss's egg [19]. The model geometry was imported to *Ansys® Academic Research Mesh, Release 22.1* (ANSYS, Inc., Canonsburg PA, USA) and discretized into an unstructured tetrahedral mesh. For the large-size egg (63–72 g), 314,029 cells were used for the discretization and the solution of the governing equations (Figure 1). The required values for the mesh used were obtained by taking into consideration the domain (fluid), the nature of the process, and the computational time required by means of mesh independence analysis. The software *Ansys® Academic Research Fluent, Release 22.1* (ANSYS, Inc., Canonsburg PA, USA) was chosen to perform the required calculations. The calculation of heat transfer and fluid flow in the proposed domain due to natural convection required numerical solution of the generalized transport equations [20].

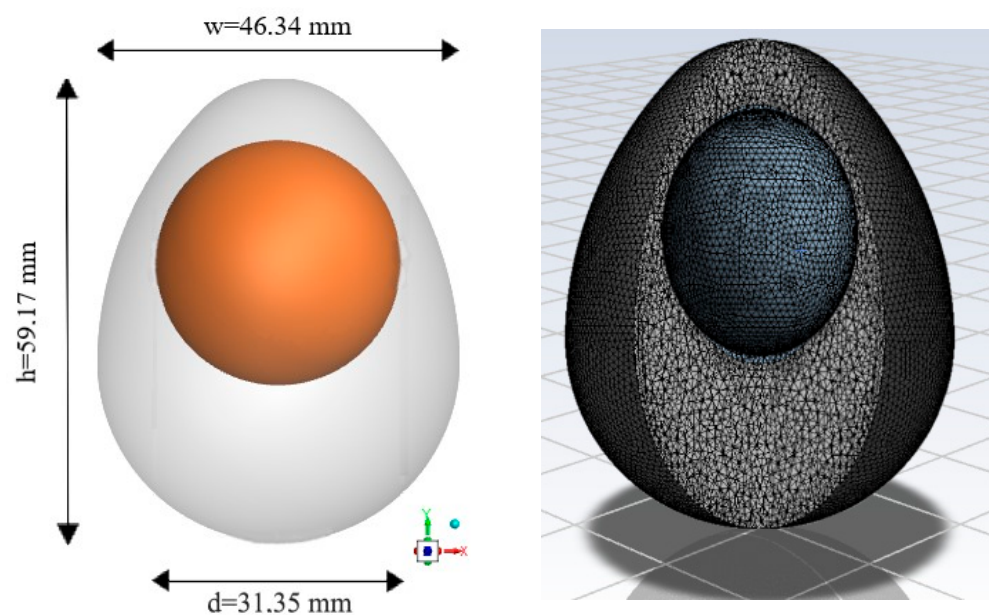


**Figure 1.** Shape and dimensions of the large-size egg used for the simulations (left) and mesh imaging (right).

The external surface of the geometry representing the eggshell was defined as a wall. The internal volume of the egg, consisting of the yolk and the albumen without any air pocket, was defined as the fluid. A membrane around the yolk was used to not allow for mass exchange between the yolk and the albumen, and it was modeled as a wall with properties identical to yolk properties. All materials used were assumed to be homogenous and isotropic. Uniform initial conditions were used. A constant medium temperature and a given experimental heat transfer coefficient was applied to the external surface of the egg. External forces, moisture transfer, and viscous dissipation were neglected. The gravitational force was set to  $g = 9.81 \text{ m/s}^2$ . A constant time step of 1 s was used to solve the transient process. The convergence criterion was set to be lower than  $10^{-6}$ .

For the design of egg geometry, fresh, large-size eggs, 63–72 g, were purchased from a local market (Athens, Greece). All eggs were examined macroscopically (ovoscopy), with the aid of a light source, for cracks and other shell defects and to determine the position of the yolk and the air pocket. At the same time, the shape of the eggs was evaluated in terms of their axial symmetry. Their weight (through a precision balance, MARK 2200, BEL Engineering<sup>®</sup>, Monza, Italy), volume (through a 500 mL volumetric cylinder) and dimensions (width and height by means of a micrometer with 25–75 mm range) were determined prior to processing. These observations and the average values of the above measurements were used for the design of the large-size egg geometry, which was subsequently used for the CFD simulations and model validation (Figure 1). Specifically, following Moss's egg design, egg height was 0.05917 m, egg width was 0.04634 m, yolk diameter was 0.03135 m, yolk distance from the bottom of the egg was 0.03559 m, and egg volume was  $6.4109 \times 10^{-5} \text{ m}^3$ . The terms “large” or “large size” egg are used throughout this paper when referring to the egg designed with the particular geometry and dimensions just presented. In order to study the effect of egg size, two additional egg sizes were designed: one corresponding to medium-size eggs (53–62 g) and one for extra-large-size eggs (>72 g), as defined by the European Regulation (EC) No 589/2008 marketing standards for eggs [21]. For the medium-size egg, egg height was 0.05500 m, egg width was 0.04594 m, yolk diameter was 0.03035 m, yolk distance from the bottom of the egg was 0.03559 m, and egg volume was  $5.7009 \times 10^{-5} \text{ m}^3$  (termed “medium” or “medium size” egg). For the extra-large egg, egg height was 0.06127 m, egg width was 0.04774 m, yolk diameter was 0.031995 m, yolk distance from the bottom of the egg was 0.03559 m, and egg volume was  $7.0666 \times 10^{-5} \text{ m}^3$  (termed “extra-large” or “extra-large size” egg). For the medium and the extra-large-size eggs, 285,818 and 347,517 cells, respectively, were used for the discretization and the solution of the governing equations. The thermophysical properties of the various egg components used for the CFD simulations are presented in Table 1. They were either treated as constants or as functions of temperature.

**Table 1.** Thermophysical properties of the various egg components used for the CFD.

Property (Units)	Egg Component	Value/Equation <sup>1</sup>	Reference
Density ( $\rho$ ) (kg/m <sup>3</sup> )	Egg white	1048	[22]
	Yolk	1035	[22]
	Shell	2300	[16]
Specific heat ( $C_p$ ) (J/kg·K)	Egg white	3560	[22]
	Yolk	3560	[22]
	Shell	888	[15]
Thermal conductivity ( $k$ ) (W/m·K)	Egg white	$0.43 + 0.00055 \times T$	[22]
	Yolk	0.337	[22]
	Shell	2.25	[15]
Viscosity ( $\mu$ ) (Pa·s)	Egg white	$3.12 - 0.0089 \times T$	[22]
	Yolk	$1.60 - 0.0048 \times T$	[22]
	Shell	-	-

<sup>1</sup> T in Kelvin.

### 2.1. Convective Heat Transfer Coefficient

The convective heat transfer coefficients between the heating or cooling medium and the egg surface were a direct input for the CFD simulation. In a rather straightforward application, a convective heat transfer coefficient between a fluid and a solid particle can be determined using the lumped capacity method, that is, by measuring the temperature evolution within a simulating solid of high conductivity with geometry similar to the actual

solid particle [23]. In our case, the convective heat transfer coefficients were experimentally determined using an aluminum sphere. For high-conductivity materials, where the internal resistance to heat transfer is negligible, an energy balance yields [24]

$$mC_p \frac{dT}{dt} = A(T - T_\infty) \quad (1)$$

which gives

$$\frac{T - T_\infty}{T_{IT} - T_\infty} m = e^{\frac{-hA}{mC_p} t} \quad (2)$$

where  $m$  is the mass of the product (kg),  $C_p$  is the specific heat of the product (J/kg·K),  $A$  is the heat transfer area (m<sup>2</sup>),  $T$  is the product temperature (°C) at time  $t$  (s),  $T_{IT}$  is the initial product temperature (°C),  $T_\infty$  is the medium temperature (°C), and  $h$  is the convective heat transfer coefficient between the heating or cooling medium and the product ((W/(m<sup>2</sup>K)).

Through Equation (2), and by monitoring the temperature at the center of the aluminum sphere during the process,  $h$  was calculated from the slope of the  $\ln[(T - T_\infty)/(T_{IT} - T_\infty)]$  vs.  $t$  straight line, fitted to the experimental data, as

$$h = \text{slope} \cdot \frac{mC_p}{A} \quad (3)$$

The experiments were conducted as described for the model validation experiments. They were performed in duplicate for heating and cooling medium temperatures of about 57 °C and 20 °C, respectively, and initial product temperatures equal to or about 24 °C and 57 °C during the heating and the cooling experiments, respectively. The mass and diameter of the aluminum sphere were 39.24 g and 31.65 mm (yielding  $A = 0.003147$  m<sup>2</sup>), respectively, measured as described for the model validation experiments, while the specific heat of the aluminum sphere was taken to be equal to 900 J/(kg·K) [25].

## 2.2. Validation Experiments

To validate the proposed CFD procedure, temperature predictions were compared with experimentally measured values. Type K thermocouples (OMEGA<sup>®</sup>, Norwalk, CT, USA) connected to a portable data logger (OM-SQ2020, 2F8mk2, OMEGA<sup>®</sup>, Norwalk, CT, USA) were used for temperature measurements (every 1 s) for both the heating and the cooling medium and inside of the egg.

To measure the temperature inside of an egg, a small hole was opened in the upper part of the egg using a sharp object. From this hole, the thermocouple was placed inside of the egg. Experiments were performed with the thermocouple being placed either at the center of the egg (approximately) or at different off-center positions. After inserting the thermocouple, the hole was sealed with a thermostable (up to 120 °C) silicone paste applied with a thermal welding pistol for silicone rods. To determine the exact position of the thermocouple, after the end of the experiment the egg was boiled so that its interior was solidified [11]. Appropriate cutting of the solid egg allowed for the determination of the location of the thermocouple. The heating process was carried out in still mode, in a 22 L water–oil bath (ONE 22, Memmert<sup>®</sup>, Schwabach, Germany), while for the cooling process a second identical water bath with a constant flow type circulator (Digiterm 100, Selecta<sup>®</sup>, Barcelona, Spain) and a cooling apparatus (Peltier CDP 115, Memmert<sup>®</sup>, Schwabach, Germany) was used.

### 2.3. Thermal Process Calculations

Thermal process calculations followed the classical thermobacteriological approach, as depicted here, with the fundamental equation for the  $F$  value [26].

$$F_{T_{ref}}^z = \int_{t=0}^{t=t_p} 10^{\frac{T(t) - T_{ref}}{z}} dt = D_{T_{ref}} (\log(C_0) - \log(C)) \quad (4)$$

where  $t_p$  is the total processing time (i.e., including both heating and cooling, min),  $T_{ref}$  is an appropriate selected reference temperature ( $^{\circ}\text{C}$ ),  $D_T$  is the decimal reduction time (min) at temperature  $T$  ( $^{\circ}\text{C}$ ),  $z$  is the temperature difference required for a change by a factor of 10 of the  $D_T$  value ( $^{\circ}\text{C}$ ),  $C$  is the concentration at time  $t$ , and  $C_0$  is the initial concentration of the microbial population or any other thermolabile substance (e.g., number of microorganisms/mL).

Based on the CFD product temperature predictions throughout the volume of the egg, the  $F$  value of each examined egg pasteurization process ( $F_{process}$ ) was calculated through the integral of Equation (4). A User-Defined Function (UDF) was written and incorporated into the CFD procedure for such calculations. The critical point of the egg, defined as the point inside of the product that receives the least effects as far as microbial destruction or destruction of any other undesirable agent is concerned, of the thermal treatment was determined based on the  $F$  value distribution at the end of the pasteurization process, revealed through the CFD calculations.

The right-hand side of Equation (4) is generally used to define the required  $F$  value ( $F_{required}$ ) [27]. For egg pasteurization, a thermal treatment for a 5-log destruction of the *Salmonella enteritidis* population [2], characterized by  $z = 4.1$   $^{\circ}\text{C}$  and  $D_{60^{\circ}\text{C}} = 0.17$  min [28], yields an  $F_{required}$  value of 0.85 min:

$$F_{60^{\circ}\text{C}}^{4.1^{\circ}\text{C}} = 5 \cdot 0.17 = 0.85 \text{ min} \quad (5)$$

For each medium temperature examined, the required heating time,  $B$  (min), to achieve the required  $F$  value at the critical point, as suggested by Equation (6), was determined through a trial-and-error procedure, with a 0.1 min accuracy.

$$F_{60^{\circ}\text{C}}^{4.1^{\circ}\text{C}} = \int_{t=0}^{t=B} 10^{\frac{T(t) - 60}{4.1}} dt + \int_{t=B}^{t=t_p} 10^{\frac{T(t) - 60}{4.1}} dt = 0.85 \quad (6)$$

During such calculations, the distinct contribution of each cycle of the pasteurization process to the total  $F$  value ( $F_{total}$ ), that is, the heating ( $F_{heating}$ ) and the cooling ( $F_{cooling}$ ) cycle  $F$  values, as suggested by the first and the second integral of Equation (6), respectively, was recorded, enabling calculations of the relative contribution of each process cycle to the total lethality.

### 2.4. Quality Degradation

For quality retention calculations, Equation (4) was solved for  $C/C_0$ :

$$\frac{C}{C_0} \times 100 = 10^{\frac{-\int_{t=0}^{t=t_p} 10^{\frac{T(t) - T_{ref}}{z}} dt}{D_{T_{ref}}}} \times 100 \quad (7)$$

Because no specific  $D$  and  $z$  values were found for quality characteristics (including nutrients) of shell eggs, quality degradation calculations were based on general thermal inactivation kinetic parameters reported for quality attributes [29]. In particular,  $D_{121.11^\circ\text{C}}$  of 100 and 1000 min coupled with  $z$  values of 20 and 50 °C were used. Concentration calculations at each node point in the egg were calculated through a Custom Field Function (Equation (7)) after point quality  $F$  value calculations (the integral appearing on Equation (7)) through the forementioned UDF. Average concentration values (% retention) were thereafter provided using built-in CFD calculations.

### 3. Results and Discussion

The following paragraphs present the results obtained during pasteurization (heating and cooling) for three different sizes of whole eggs. Initially, egg pasteurization CFD simulations were compared with experimental data to evaluate the model and define the critical point inside of the examined eggs. Subsequently, the  $F$  value for *Salmonella enteritidis* and quality factors were obtained via the CFD to assess the eggs' pasteurization process for safety and quality.

#### 3.1. Convective Heat Transfer Coefficient

Based on the experimental temperature data at the center of the aluminum sphere (Figure 2a), the convective heat transfer coefficient between the heating medium and the egg surface was calculated as equal to 644 W/(m<sup>2</sup>K). For the cooling cycle (Figure 2b), the corresponding value was equal to 1289 W/(m<sup>2</sup>K). It is interesting to note that due to water circulation, the heat transfer coefficient during the cooling cycle was double the respective value of the heating cycle. These heat transfer coefficient values were subsequently used in the CFD runs.

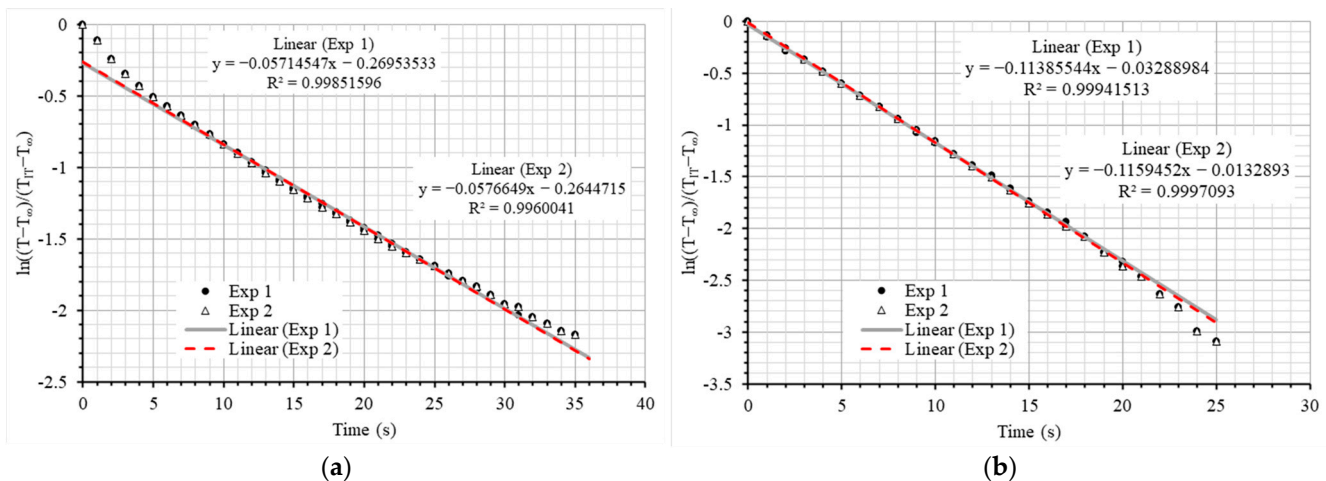


**Figure 2.** Determination of the convective heat transfer coefficients between the heating (a) and the cooling (b) medium and the egg surface (from two experiments, Exp 1 and Exp 2, for each case).

#### 3.2. Validation Experiments

Comparisons between temperature predictions and experimental data are presented in Figures 3 and 4 for a number of individual large-size eggs at different positions inside of the eggs. Figure 3 shows an example of temperature comparisons for the whole pasteurization process at the geometric center of the egg, i.e., at point (0, 0.0296, 0). Note that the (0, 0, 0), coordinate point (x, y, z) was taken on the axis of symmetry at the bottom of the egg, and coordinates reported here are in meters. Figure 4 refers to comparisons between predicted and experimental unaccomplished temperature ratios during heating at the geometric center, point B (0, 0.0296, 0), of five different large-size eggs, and at an off-center

position, A (0.0070, 0.0296, 0), at approximately half of the distance between the center and the surface of a large-size egg. Comparing the unaccomplished temperature ratios  $[(T_{\infty}-T)/(T_{\infty}-T_{IT})]$  permits comparisons between cases where the initial egg temperature ( $T_{IT}$ ) or the heating medium temperature ( $T_{\infty}$ ) differs between replicate experiments. The agreement between predicted and experimental temperature data was satisfactory, allowing for further calculations using the developed CFD code with the chosen egg geometry, mesh quality, thermophysical properties, and heat transfer coefficients.

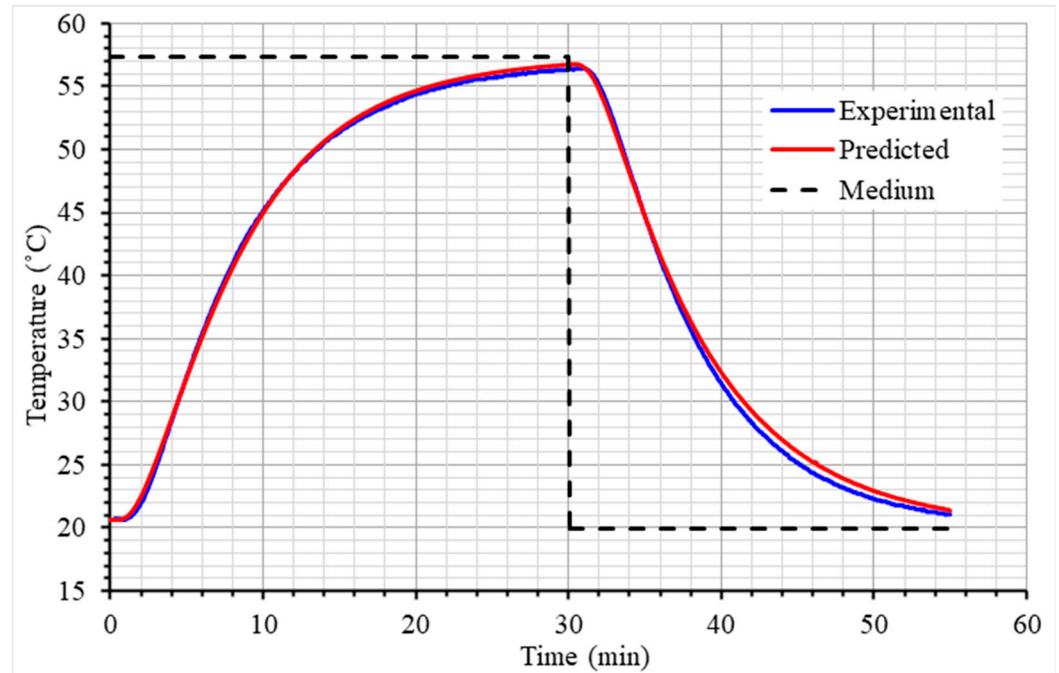


**Figure 3.** Comparison between predicted and experimental temperature evolution data during heating and cooling of large-size egg.

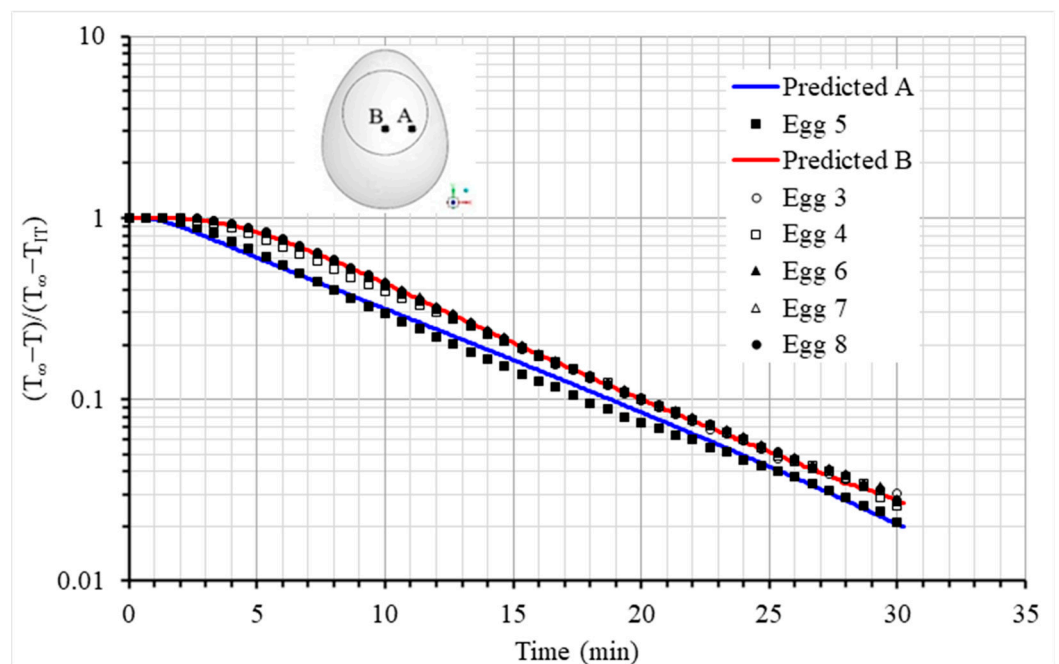


**Figure 4.** Comparison between predicted and experimental unaccomplished temperature ratios at different positions, A and B, of the egg’s interior during heating of individual large-size eggs.

### 3.3. Thermal Process Calculations

Typical temperature distribution evolutions for the large-size egg during 29.1 min of heating at 58 °C and 25.0 min of cooling at 20 °C, at vertical and horizontal cross-sections, are presented in Figures 5 and 6, respectively. Corresponding *F* value distributions are depicted in Figure 7.

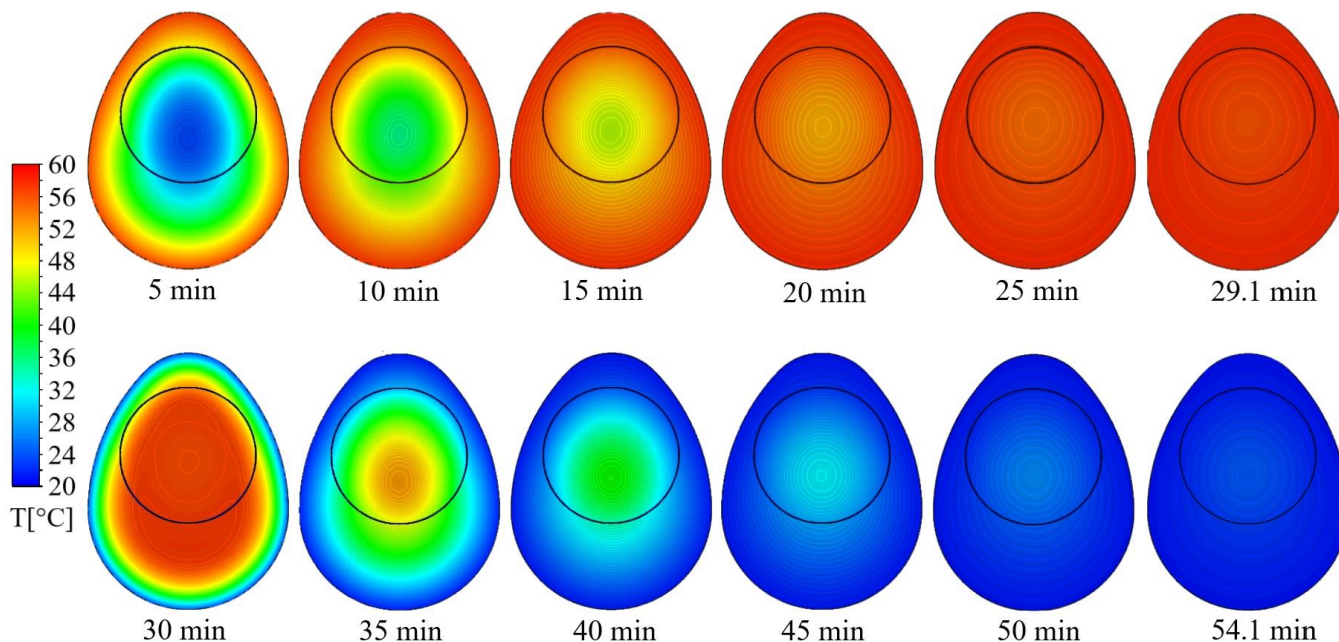


**Figure 5.** Evolution of temperature distribution, vertical cross-section, for the large-size egg during 29.1 min of heating at 58 °C and 25.0 min of cooling at 20 °C.

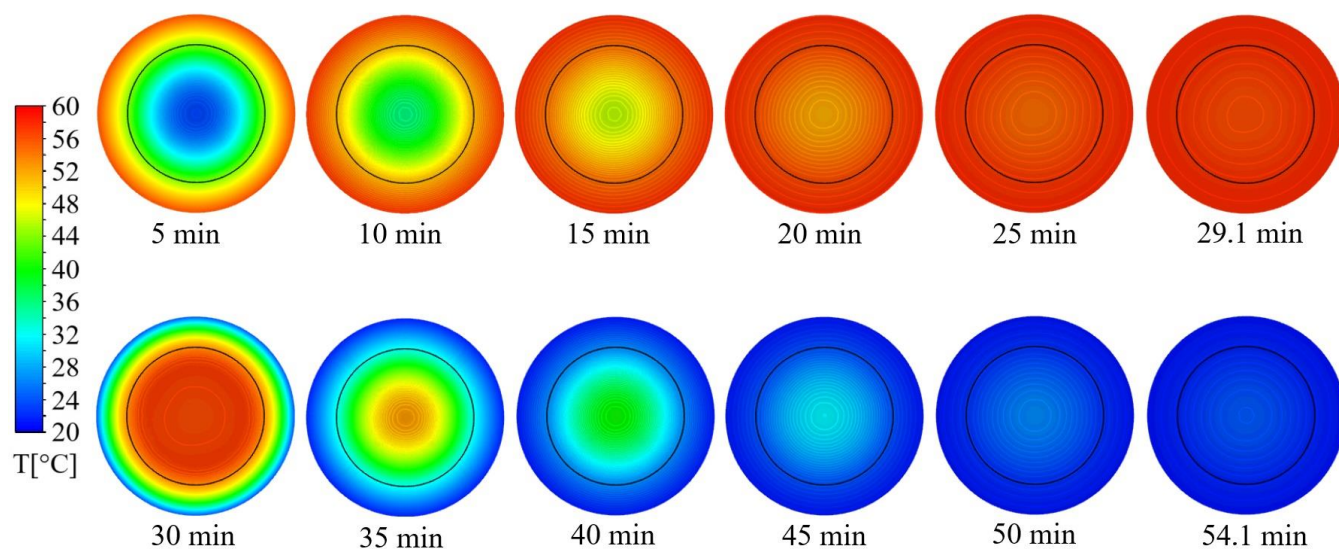


**Figure 6.** Evolution of temperature distribution, horizontal cross-section, for the large-size egg during 29.1 min of heating at 58 °C and 25.0 min of cooling at 20 °C.

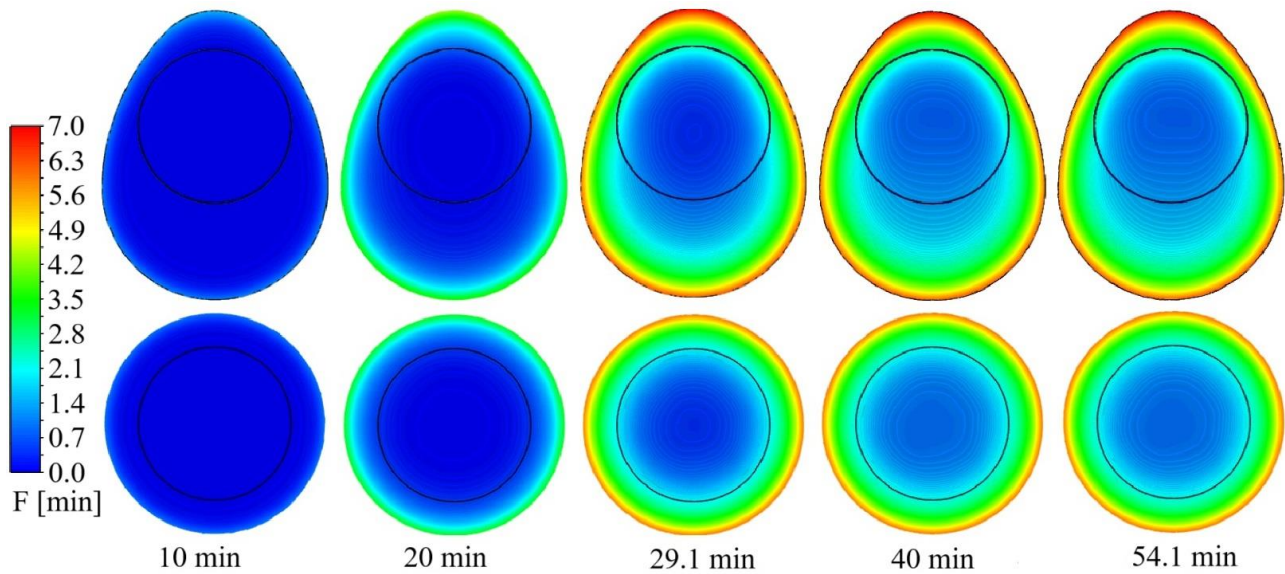


**Figure 7.** Evolution of the  $F$  value distribution, horizontal and vertical cross-sections, for the large-size egg during 29.1 min of heating at 58 °C and 25.0 min of cooling at 20 °C.

Based on the  $F$  value distribution at the end of the entire process, the critical point was determined, as presented in Figure 8 for the large-size egg heated at 58 °C. For the same target  $F$  value, the critical point was somewhat displaced depending on the heating medium temperature, presumably a result of the cooling cycle. More specifically, for a medium temperature of 54 °C, it was located at  $x = 0.0023$ ,  $y = 0.0360$ , and  $z = -0.0019$ ; for 56 °C, it was located at  $x = 0.0019$ ,  $y = 0.0365$ , and  $z = -0.0012$ ; for 58 °C, it was located at  $x = 0.0021$ ,  $y = 0.03754$ , and  $z = -0.0010$ ; and for 60 °C, it was located at  $x = 0.0013$ ,  $y = 0.0387$ , and  $z = -0.0011$ . That is, the critical point was moving slightly upwards as medium temperature increased.

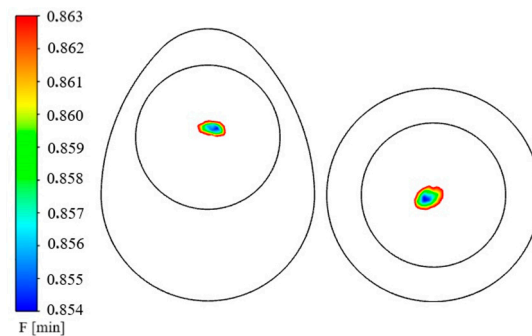


**Figure 8.** Determination of the critical point at the end of the pasteurization process, i.e., for  $F_{60^{\circ}\text{C}}^{4.1^{\circ}\text{C}} = 0.85$  min, for the large-size egg during 29.1 min of heating at 58 °C and 25.0 min of cooling at 20 °C.

The required heating time to achieve an  $F_{60^{\circ}\text{C}}^{4.1^{\circ}\text{C}} = 0.85$  min, together with the  $F_{heating}$  and  $F_{cooling}$  values, were determined through a trial and error procedure for the medium, large, and extra-large-size egg for each medium temperature examined, that is, for 54 °C, 56 °C, 58 °C, and 60 °C (Table 2). For the large-size eggs, heating times were 24.5, 29.1, 37.2, and 55.1 min for medium temperatures of 60 °C, 58 °C, 56 °C, and 54 °C, respectively. The required heating times for each egg size, medium, large, and extra-large, for each medium temperature are presented in Table 2. Temperature evolution data at the critical point during large egg pasteurization at different medium temperatures are presented in Figure 9.  $F$  value evolution at the critical point during large egg pasteurization at different

medium temperatures is presented in Figure 10. Note that for the same egg size, as the medium temperature increases, the contribution of cooling to the total lethality increases (Table 2). Similarly, as the egg size increases, the contribution of cooling to the total lethality also increases (Table 2). As far as quality is concerned, retention values ranged between 94.22 and 100.00%, which means that thermal pasteurization does not cause real quality problems, at least for the typical kinetic parameters employed (Table 3).

**Table 2.** Required heating times,  $B$ , for a target  $F_{60^{\circ}\text{C}}^{4.1^{\circ}\text{C}}$  value of 0.85 min ( $F_{total}$ ), together with the  $F_{heating}$  and  $F_{cooling}$  values, during egg pasteurization in different time and temperature conditions.

Egg Size	Heating Medium $T$ ( $^{\circ}\text{C}$ )	Heating Time $B$ (min)	$F_{total}$ (min)	$F_{heating}$ (min)	$F_{cooling}$ (min)	% Contribution of Cooling Lethality
Medium	54	53.1	0.85	0.75	0.10	11.8
	56	35.5	0.85	0.62	0.23	27.1
	58	27.8	0.86	0.49	0.37	43.5
	60	23.4	0.86	0.41	0.45	52.9
Large	54	55.1	0.85	0.74	0.11	13.0
	56	37.2	0.86	0.6	0.26	29.9
	58	29.1	0.86	0.46	0.40	46.2
	60	24.5	0.86	0.32	0.53	62.3
Extra Large	54	56.8	0.85	0.71	0.14	16.5
	56	38.8	0.86	0.54	0.32	37.6
	58	30.5	0.86	0.37	0.49	57.6
	60	25.8	0.87	0.25	0.62	72.9

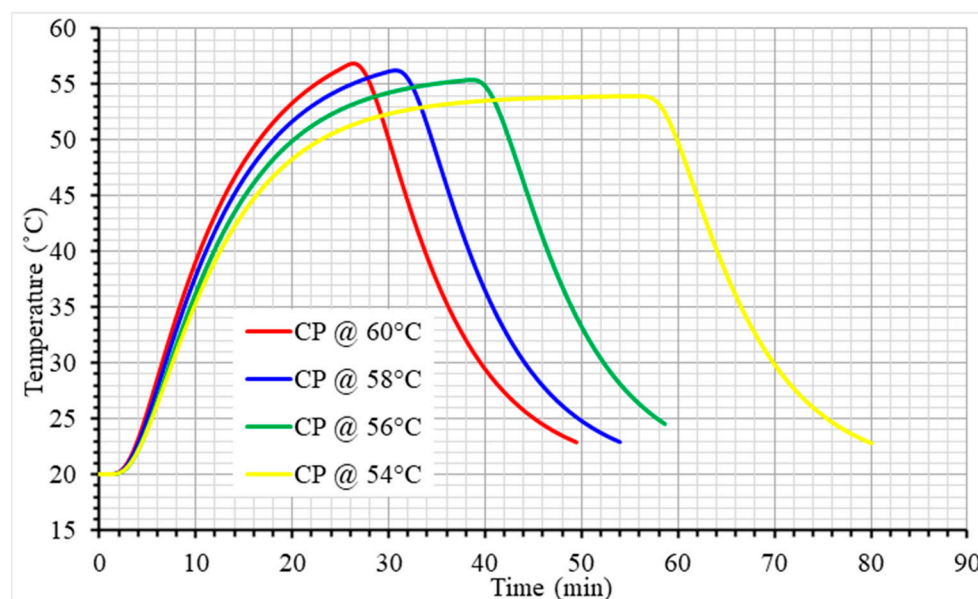


**Figure 9.** Temperature evolution at the critical point (CP) during large-size egg pasteurization, for processes targeting  $F_{60^{\circ}\text{C}}^{4.1^{\circ}\text{C}} = 0.85$  min at different medium temperatures (@ 54, 56, 58, and 60  $^{\circ}\text{C}$ ).

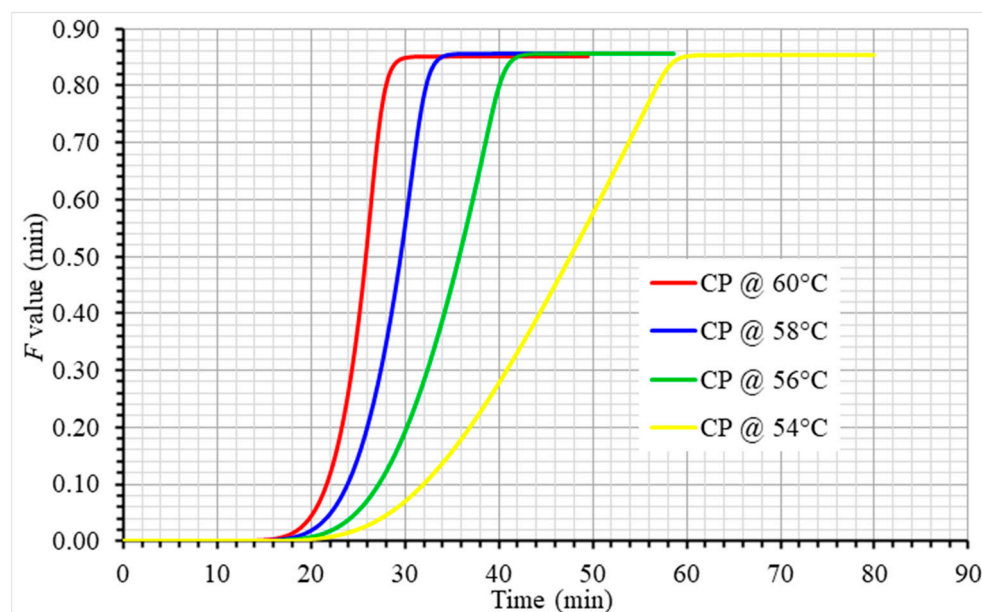


**Figure 10.**  $F_{60^{\circ}\text{C}}^{4.1^{\circ}\text{C}}$  value evolution at the critical point (CP) during large-size egg pasteurization, for processes targeting  $F_{60^{\circ}\text{C}}^{4.1^{\circ}\text{C}} = 0.85$  min at different medium temperatures (@ 54, 56, 58, and 60 °C).

**Table 3.** Retention of quality attributes, characterized by different  $D$  and  $z$  values, during large-size egg pasteurization in different time and temperature conditions.

Heating Medium $T$ (°C)	Heating Time $B$ (min)	$D_{121.11^{\circ}\text{C}}$ (min)	$z$ (°C)						
		100	20	1000	20	100	50	1000	50
54	55.1	99.95		100.00		94.22		99.41	
56	37.2	99.96		100.00		95.77		99.57	
58	29.1	99.97		100.00		96.34		99.63	
60	24.5	99.97		100.00		96.67		99.66	

#### 4. Conclusions

The required heating times, at several different heating medium temperatures and for three different egg sizes, were estimated using CFD simulation. Calculations were performed for a 5-log reduction of the *Salmonella enteritidis* population at the critical point of the eggs. Model predictions of the temperature history of internal egg points were in good agreement with experimental data. The critical point location, approximately at the center of the yolk, was assessed through  $F$  value distribution calculations. Microbial destruction occurring during the cooling cycle of the pasteurization process was considerable and should not be ignored during process design, as it can lead to unnecessarily long heating times. Cooling lethality ranged between 11.8% for the medium-size egg processed at 54 °C and 72.9% for the extra-large-size egg processed at 60 °C of the total destruction. Finally, quality degradation was minimal during thermal pasteurization, allowing for process optimization based on different criteria, including cycle time, productiveness, and energy costs.

**Author Contributions:** Conceptualization, N.G.S.; methodology, N.G.S. and S.M.C.; software, P.-A.S., S.M.C. and G.N.S.; validation, G.N.S.; formal analysis, P.-A.S. and S.M.C.; investigation, P.-A.S.; data curation, P.-A.S., S.M.C. and G.N.S.; writing—original draft preparation, P.-A.S., S.M.C. and G.N.S.; writing—review and editing, S.M.C. and N.G.S.; visualization, N.G.S.; supervision, N.G.S.; project administration, N.G.S. All authors have read and agreed to the published version of the manuscript.

**Funding:** This research received no external funding.

**Data Availability Statement:** The original contributions presented in this study are included in the article. Further inquiries can be directed to the corresponding author.

**Conflicts of Interest:** The authors declare no conflicts of interest.

## Nomenclature

$A$	heat transfer area, $m^2$
$B$	required heating time, min
$C$	concentration of a heat labile substance, number of microorganisms/mL, spores per container, g/mL, or any other appropriate unit
$C_p$	specific heat of the product, J/(kg·K)
$D_T$	(noted also as $D$ ) decimal reduction time or death rate constant—time at a constant temperature required to reduce by 90% the initial spore load (or, in general, time required for 90% reduction of a heat labile substance), min
$m$	mass, kg
$F_T^z$	(or simply $F$ ) time at a constant temperature, $T$ , required to destroy a given percentage of microorganisms whose thermal resistance is characterized by $z$ , or the equivalent processing time of a hypothetical thermal process at a constant temperature that produces the same effect (in terms of spore destruction) as the actual thermal process, min
$h$	convective heat transfer coefficient between the heating or cooling medium and the product, $W/(m^2K)$
$T$	product temperature, $^{\circ}C$
$t$	time, s or min
$x, y, z$	orthogonal coordinates
$z$	temperature difference required to achieve a decimal change of the $D_T$ value, $^{\circ}C$
<i>Subscripts</i>	
cooling	referring to the cooling cycle
heating	referring to the heating cycle
$IT$	initial condition
$p$	process
process	process value
required	required value
total	cumulative value
$\infty$	heating or cooling medium

## References

- Rehault-Godbert, S.; Guyot, N.; Nys, Y. The golden egg: Nutritional value, bioactivities, and emerging benefits for human health. *Nutrients* **2019**, *11*, 684. [[CrossRef](#)] [[PubMed](#)]
- FDA. 21 CFR Parts 16 and 118. Prevention of *Salmonella enteritidis* in Shell Eggs During Production, Storage, and Transportation. *Fed. Regist.* **2009**, *74*, 33030–33101.
- Li, L.; McWhorter, A.; Chousalkar, K. Ensuring egg safety: Salmonella survival, control, and virulence in the supply chain. *Compr. Rev. Food Sci. Food Saf.* **2025**, *24*, e70075. [[CrossRef](#)] [[PubMed](#)]
- Gantois, I.; Ducatelle, R.; Pasmans, F.; Haesebrouck, F.; Gast, R.; Humphrey, T.J.; Immerseel, F.V. Mechanisms of egg contamination by *Salmonella enteritidis*. *FEMS Microbiol. Rev.* **2009**, *33*, 718–738. [[CrossRef](#)] [[PubMed](#)]
- Keener, K. Shell Egg Pasteurization. In *Egg Innovations and Strategies for Improvements*; Hester, P.Y., Ed.; Elsevier: Amsterdam, The Netherlands; Academic Press: Cambridge, MA, USA, 2017; pp. 165–175. [[CrossRef](#)]
- Ebel, E.; Schlosser, W. Estimating the annual fraction of eggs contaminated with *Salmonella enteritidis* in the United States. *Int. J. Food Microbiol.* **2000**, *61*, 51–62. [[CrossRef](#)] [[PubMed](#)]
- EFSA, European Food Safety Authority and the European Centre for Disease Prevention and Control. The European Union One Health 2018 Zoonoses Report. *EFSA J.* **2019**, *17*, 5926. [[CrossRef](#)]

8. EFSA, European Food Safety Authority and the European Centre for Disease Prevention and Control. Multi-country outbreak of *Salmonella enteritidis* sequence type (ST)11 infections linked to eggs and egg products. *EFSA Support. Publ.* **2022**, *19*, 7180E. [[CrossRef](#)]
9. FSN. Food Safety News: *Salmonella* Outbreak in Sweden Linked to Eggs. Available online: <https://www.foodsafetynews.com/2023/01/salmonella-outbreak-in-sweden-linked-to-eggs/> (accessed on 24 January 2023).
10. Abbasnezhad, B.; Hamdami, N.; Shahedi, M.; Vatankhah, H. Thermophysical and rheological properties of liquid egg white and yolk during thermal pasteurization of intact eggs. *Food Meas. Charact.* **2014**, *8*, 259–269. [[CrossRef](#)]
11. Abbasnezhad, B.; Hamdami, N.; Monteau, J.Y.; Vatankhah, H. Numerical modeling of heat transfer and pasteurizing value during thermal processing of intact egg. *Food Sci. Nutr.* **2015**, *4*, 42–49. [[CrossRef](#)] [[PubMed](#)]
12. Bermudez-Aguirre, D.; Niemira, B.A. A review on egg pasteurization and disinfection: Traditional and novel processing technologies. *Compr. Rev. Food Sci. Food Saf.* **2022**, *22*, 756–784. [[CrossRef](#)] [[PubMed](#)]
13. Hou, H.; Singh, R.K.; Muriana, P.M.; Stadelman, W.J. Pasteurization of intact shell eggs. *Food Microbiol.* **1996**, *13*, 93–101. [[CrossRef](#)]
14. Schuman, J.D.; Sheldon, B.W.; Vandepopuliere, J.M.; Ball, H.R., Jr. Immersion heat treatments for inactivation of salmonella enteritidis with intact eggs. *J. Appl. Microbiol.* **1997**, *83*, 438–444. [[CrossRef](#)] [[PubMed](#)]
15. Denys, S.; Pieters, J.G.; Dewettinck, K. Computational fluid dynamics analysis of combined conductive and convective heat transfer in model eggs. *J. Food Eng.* **2004**, *63*, 281–290. [[CrossRef](#)]
16. Denys, S.; Pieters, J.G.; Dewettinck, K. Computational fluid dynamics analysis for process impact assessment during thermal pasteurization of intact eggs. *J. Food Prot.* **2005**, *68*, 366–374. [[CrossRef](#)] [[PubMed](#)]
17. Park, H.W.; Yoon, W.B. Computational fluid dynamics (CFD) modelling and application for sterilization of foods: A Review. *Processes* **2018**, *6*, 62. [[CrossRef](#)]
18. Szpicer, A.; Bińkowska, W.; Stelmasiak, A.; Zalewska, M.; Wojtasik-Kalinowska, I.; Piwowarski, K.; Piepiórka-Stepuk, J.; Półtorak, A. Computational fluid dynamics simulation of thermal processes in food technology and their applications in the food industry. *Appl. Sci.* **2025**, *15*, 424. [[CrossRef](#)]
19. Dixon, R. *Mathographics*; Dover Publications Inc.: Mineola, NY, USA, 1991; pp. 3–11.
20. Sun, D.W. *Computational Fluid Dynamics in Food Processing*; CRC Press/Taylor & Francis Group: Boca Raton, FL, USA, 2007; p. 760.
21. European Commission. Commission Regulation (EC) No. 589/2008 of 23 June 2008 laying down detailed rules for implementing Council Regulation (EC) No. 1234/2007 as regards marketing standards for eggs. *Off. J. Eur. Union (EN)* **2008**, *50*, 6–23.
22. Romanoff, A.; Romanoff, A. *The Avian Egg*; John Wiley and Sons, Inc.: New York, NY, USA, 1949.
23. Badin, E.E.; Mercatante, M.M.; Mascheroni, R.H.; Quevedo-Leon, R.; Ibarz, A.; Ribotta, P.D.; Lespinard, A.R. Effect of pasteurization on color, ascorbic acid and lycopene of crushed tomato: A computational study with experimental validation. *J. Food Eng.* **2023**, *337*, 111218. [[CrossRef](#)]
24. Heldman, D.R.; Singh, R.P. *Food Process Engineering*, 2nd ed.; The AVI Publishing Company, Inc.: Baton Rouge, LA, USA, 1981; p. 481.
25. ASM Handbook Committee. *ASM Handbook Volume 2, Properties and Selection: Nonferrous Alloys and Special-Purpose Materials*, 10th ed.; ASM International/The Materials Information Company: Russell Township, OH, USA, 1990.
26. Ball, C.O.; Olson, F.C.W. *Sterilization in Food Technology. Theory, Practice and Calculations*; McGraw-Hill Book Co.: New York, NY, USA, 1957.
27. Stoforos, N.G. Thermal Processing. In *Handbook of Food Processing: Food Preservation*; Varzakas, T., Tzia, C., Eds.; CRC Press/Taylor & Francis Group: Boca Raton, FL, USA, 2015; pp. 27–56.
28. Jin, T.; Zhang, H.; Boyd, G.; Tang, J. Thermal resistance of *Salmonella enteritidis* and *Escherichia coli* K12 in liquid egg determined by thermal-death-time disks. *J. Food Eng.* **2008**, *84*, 608–614. [[CrossRef](#)]
29. Lund, D.B. Design of thermal processes for maximizing nutrient retention. *Food Technol.* **1977**, *31*, 71–78.

**Disclaimer/Publisher’s Note:** The statements, opinions and data contained in all publications are solely those of the individual author(s) and contributor(s) and not of MDPI and/or the editor(s). MDPI and/or the editor(s) disclaim responsibility for any injury to people or property resulting from any ideas, methods, instructions or products referred to in the content.